Proceedings of ISFOG 2025
5TH INTERNATIONAL SYMPOSIUM ON
FRONTIERS IN OFFSHORE GEOTECHNICS
Nantes, France | June 9-13 2025
© 2025 the Authors
ISBN 978-2-85782-758-0

Behaviour of a reverse T-shape anchor subjected to horizontal loading in sand

Pierre-Yves Duverneuil*
Norwegian Geotechnical Institute (NGI), Perth, Australia

Muhammad Shazzad Hossain
Centre for Offshore Foundation Systems (COFS) / The University of Western Australia, Perth, Australia

Henning Mohr
MSMT Solutions (MSMT) / Perth, Australia

Yun Sup Shin
Norwegian Geotechnical Institute (NGI), Oslo, Norway

**pierre.yves.duverneuil@ngi.no (corresponding author)*

ABSTRACT: Drag or suction embedded plate anchors are widely recognised as an efficient anchoring solution for mooring offshore floating wind turbines, wave energy converters, solar panels, and aquaculture cages. This paper reports the performance of a reverse T-shape plate anchor concept in sand. Two series of tests were conducted on half- and full-model anchors in a centrifuge facility. The model anchors were pre-embedded at depths of 1.3 and 1.6 times the width of the plates in flat and 20° sloped sand deposits. A horizontal load was then applied at a height of 0.5 times the width of the plates from the soil surface.

Half-anchor tests, conducted against a window, allowed two cameras to capture soil deformation images which were subsequently quantified by particle image velocimetry analyses. Full-anchor tests, carried out inside the soil samples, were used to verify the load-displacement response from the half-anchor tests. From the combined set of experiments, displacement vectors and incremental shear strain contours were plotted linking directly to the critical points on the resistance profiles: (i) a first peak in the load-displacement response was associated predominantly with the rotational movement of the square plate (ii) a second peak, with magnitudes ranging from 2 to 3 times of that at the first peak, was associated with the plate and shaft being uplifted and translated. These observations will allow for the development of analytical solutions and mechanism-based design approaches for assessing capacity under horizontal loading.

Keywords: Centrifuge modelling, plate anchor, Particle Image Velocimetry (PIV), sand.

1 INTRODUCTION

The world energy production is transitioning from hydrocarbon (oil and gas)-based sources to renewable alternatives - such as offshore wind, wave, solar or tidal energy. Compared with oil and gas development, harvesting offshore renewable energies possesses multiple challenges, e.g. there is a huge difference in number of required foundations or anchors and installation seabed area. Each oil and gas platform is an isolated facility, and is generally supported by 3 to 4 foundations or < 20 bespoke anchors (e.g. 16 piles for the 36,112 m^2 Prelude FLNG). In contrast, development of, for example, a 1 GW offshore wind farm requires installation of 67 to 200 foundations or 200 anchors over 250 km^2 seabed area for supporting 67 turbines of 15 MW each. Therefore, cost-effective foundations and ('shared') anchoring solutions are essential for making renewable energy more competitive in the global energy market.

This paper focuses on proposing an anchoring solution for mooring floating renewable energy units (such as wind turbines, wave energy converters, solar panels) and aquaculture cages. Piles (including screw piles), suction caissons/buckets, suction embedded plate anchors, drag anchors, and dynamically installed torpedo and fish anchors can potentially be used for tethering floating facilities (Cerfontaine et al., 2023). Suction caissons and drag anchors have been utilised in the commissioning of four floating wind farms including Hywind Scotland, Windfloat Atlantic, Kincardine, Hywind Tampen (Subbulakshmi et al., 2024). This paper proposes a reverse T-shape plate anchor. This square plate anchor can potentially be shared by two or four mooring lines from multiple floating units, making it a critical innovation for the development of floating wind farms (Xu et al., 2024). The performance of the anchor under uniaxial monotonic horizontal loading in sand is reported in this paper.

2 EXPERIMENTAL DETAILS

Two series of centrifuge experiments were performed in the National Geotechnical Centrifuge Facility at the University of Western Australia, comprising (i) full-model tests within the soil samples in the 5 m radius beam centrifuge, and (ii) half-model tests against a window in the 1.8 m radius beam centrifuge. Soil samples were prepared with either a flat or 20° sloped surface.

2.1 Full-anchor experiments

The full-anchor tests were conducted at 50g. Two 1:50 scale model reverse T-shape square plate anchors, referred to as T1 and T2, were fabricated from aluminium (Figure 1a). The width (B) of the plates or at the base of the two anchors was 70 mm (represents 3.5 m in prototype scale) with a plate thickness (t) of 15 mm. The shaft diameter (d) was 24 mm. The lengths (L), measured from the plate base to the loading point, were 147 mm and 126 mm (7.4 m and 6.3 m in the field scale) for T1 and T2, respectively. The embedment depths of the base of the anchors (D) were 112 mm for T1 and 91 mm for T2, with respective normalised embedment depths being D/B = 1.6 and 1.3. The horizontal loading point (i.e. the padeye at the top of the anchor) was set at a distance of 35 mm (0.5B) above the average ground surface.

Table 1 summarises the dimensions of the model anchors.

Table 1. Dimensions of full-model and half-model anchors.

Test type	Test ID	Width[1], B	Embedment[1], D	D/B
Full-anchor	T1	70 / 3.5	112 / 5.6	1.6
Full-anchor	T2	70 / 3.5	91 / 4.55	1.3
Half-anchor	HT1	35 / 3.5	56 / 5.6	1.6
Half-anchor	HT2	35 / 3.5	45.5 / 4.55	1.3

[1](mm, model) / (m, prototype)

The experimental set-up, as shown in Figure 2a, used a linear actuator mounted perpendicular onto a platform and connected to the anchor padeye via a rope that travelled around a pulley. The anchor was loaded by controlling the vertical displacement of the actuator. The horizontal load on the anchor was measured using a 5 kN in-line load cell attached between the actuator bracket and the rope.

The anchor movement was recorded using a marker-based tracking solution (Photron, 2024). A 5-megapixel camera continuously captured images of the anchor, on which a fiducial marker was attached. Commercial software '6D Marker' provided by Photron resolved the marker position from the recorded images. Additional details on the "6D Marker" can be found in Mohr et al. (2022).

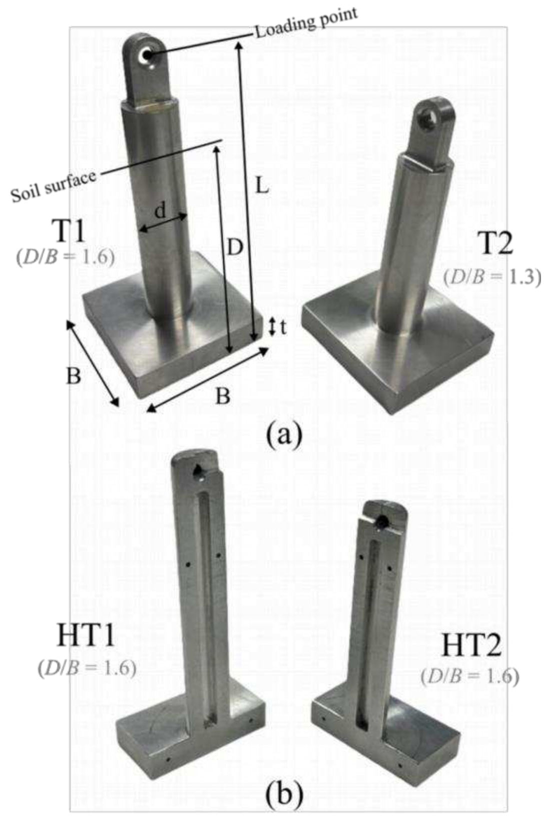

Figure 1. Model reverse T-Shape anchors: (a) full-anchors; and (b) half-anchors.

2.2 Half-anchor experiments

The half-anchor tests were conducted at 100g using two 1:100 scale model reverse T-shape half-anchors (i.e. optimal size and centrifuge acceleration to be able to fully observe the failure mechanism), referred to as HT1 and HT2 and with dimensions proportional to T1 and T2, respectively (see Table 1). To maintain the anchor model against the window during loading, a groove was cut on the shaft of the foundations and filled with petroleum jelly (grease), applying suction against the window.

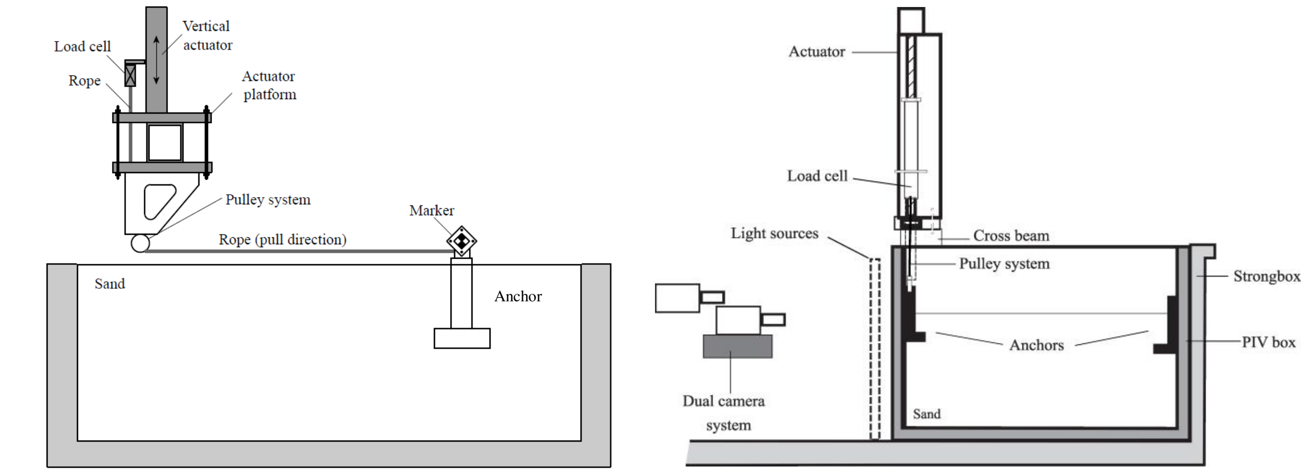

(a) (b)

Figure 2. Schematic diagram of typical experimental set-ups: (a) full-anchor tests; and (b) half-anchor tests.

The experimental set-up included a PIV strongbox that contained the soil sample and model anchors. The two long sides of the PIV strongbox consisted of 50 mm thick acrylic windows with impregnated markers, providing control points for photogrammetric corrections (conversions from image space pixel coordinates to object space millimetre coordinates accounting for lens deflection and camera movement). Schematic views of the PIV strongbox with anchor models are provided in Figure 2b. The PIV strongbox was fitted at one side of the standard beam strongbox that supported a loading apparatus and a multi-scale PIV acquisition system. A linear actuator was mounted onto the standard strongbox and connected to the anchor via a rope that traveled over a pulley system, ensuring that the horizontal load was applied similarly to the set-up in the full-anchor tests. A 2-kN load cell installed at the end of the actuator connected to the rope for measuring the load applied to the anchor.

Two 5-megapixel digital cameras synchronised with the data acquisition system were fixed on the other side of the standard strongbox at optimised distances from the PIV window to capture high resolution images during the loading events. The "wide-angle" camera provided a view of the entire domain of expected deformations, while the "zoomed-in" camera focused on the area around the anchor plate, where significant deformations were anticipated. The images were analysed by particle image velocimetry (PIV) using GeoPIV-RG (Stanier et al., 2016; Teng et al., 2017). The displacement at the loading point measured from the actuator feedback was validated by the measurements from the PIV results, ensuring measurement accuracy.

2.3 Test programme

A total of 16 tests (8 full-anchor / 8 half-anchor) were carried out across 8 strongboxes covering two anchor geometries (T1/HT1 and T2/HT2), two different sand relative densities (loose/medium dense and dense), and two different ground slopes (0° i.e. flat and 20°). Horizontal monotonic loading was applied by pulling the rope at a constant rate of 0.1 mm/s. This was to ensure drained conditions as would be the case for loading anchors in sand in the field. The tests were therefore carried out in dry sand bed.

This paper presents the results of 1 full-anchor (T2) and 1 half-anchor (HT2) tests in dense sand and with embedment ratio, $D/B = 1.3$ and flat ground surface.

2.4 Sample preparation and characterisation

Soil samples were prepared using commercially available UWA superfine silica sand, with the geotechnical properties given in Table 2. For full-model tests, the sample was prepared in a large beam centrifuge strongbox (1000 × 1000 × 500 mm) by raining sand in layers maintaining a constant drop height. For half-model tests, some sand particles were dyed to black colour. 30% dyed (black) sand was mixed thoroughly with 70% untreated (white) sand (following Stanier and White, 2013). This was to provide contrasting texture for PIV analyses. The mixed sand was then rained in the PIV strongbox (337 × 225 × 300 mm) with Perspex windows in the two opposite long sides.

Table 2. Properties of UWA superfine silica sand (after Chow et al., 2019).

Property	Notation	Value	Unit
Specific gravity	G_s	2.67	-
Particle size	D_{50}	0.18	mm
Minimum dry density	$\rho_{d,min}$	1497	kg/m^3
Maximum dry density	$\rho_{d,max}$	1774	kg/m^3
Critical state friction angle (triaxial testing)	ϕ'_c	31.9	°

During the sand raining process, the model anchors were pre-embedded at the targetted depths. Sand raining was then continued up to the designed sample depth. Pre-embedment was to isolate the test results from any effects of potential installation procedures (e.g., dragging, backfill). The final surface was levelled through vacuuming.

Samples were characterised through in-flight (at 50g for full-anchor tests and at 100g for half-anchor tests) cone penetration tests. A miniature 10 mm diameter cone was penetrated at a rate of 1 mm/s. The measured cone tip resistance (q_c) profiles are plotted in Figure 3 as a function of normalised penetration depth z/B.

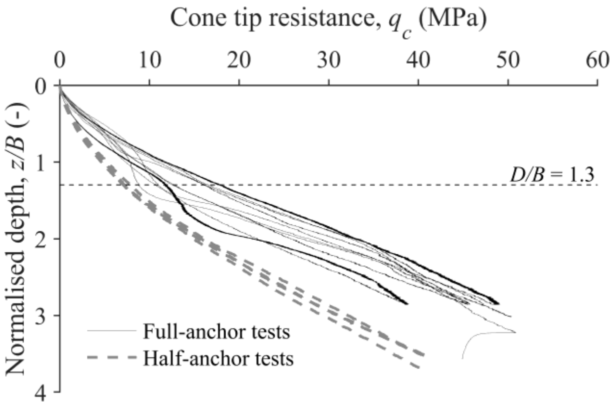

Figure 3. Profiles of cone tip resistance.

Based on the empirical formula given by Schneider & Lehane (2006) (i.e. $D_r = \sqrt{(q_c - \sigma_{v0})/(250\,\sigma'_{v0})}$, where σ_{vo} is the total vertical stress and σ'_{vo} is the effective stress), sand relative densities (D_R) were about 100 % for the full-anchor tests and 85 % for the half-anchor tests, corresponding to a dry unit weight (γ_{dry}) of 17.4 kN/m^3 and 16.9 kN/m^3, respectively.

3 RESULTS AND DISCUSSION

3.1 Load displacement responses and anchor movement

The load displacement responses for the tests are shown in Figure 4. The horizontal displacement (x) of the loading point was normalised by B. The horizontal loads were normalised by the product $\gamma_{dry} DA$, where A is the anchor base area B^2.

The profiles from the full-anchor (T2) and half-anchor (HT2) tests were reasonably consistent, exhibiting four distinct load mobilisation phases: (i) phase 1 – rising sharply with the progress of loading ($x/B \leq 0.1$), (ii) phase 2 - reaching to the 1st peak ($x/B = 0.25$) followed by a drop, (iii) phase 3 - rising slowly again, (iv) phase 4 - attaining the 2nd peak (at about $x/B = 1.5$) followed by a sharp drop or failure (though the profile for T2 did not reach this point as there was a risk of disturbance to the neighbouring test sites).

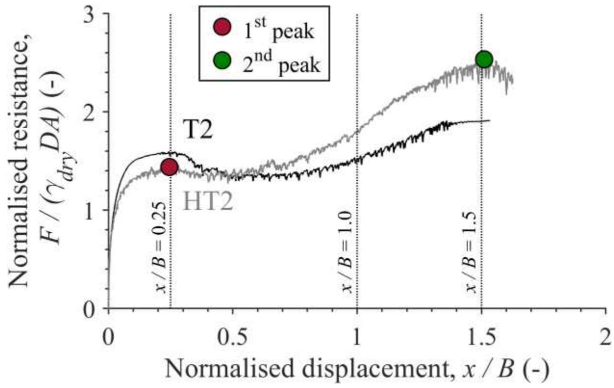

Figure 4. Normalised resistance profiles from full-anchor (T2, black) and half-anchor (HT2, grey) tests.

These four phases were associated with a combination of gradual rotation, uplift, and translation of the anchor towards the loading direction. These patterns are illustrated in Figure 5, which shows the movements of the anchor and the soil surface being tracked through the PIV technique and the use of the software Tracker (Open Source Physics, 2024).

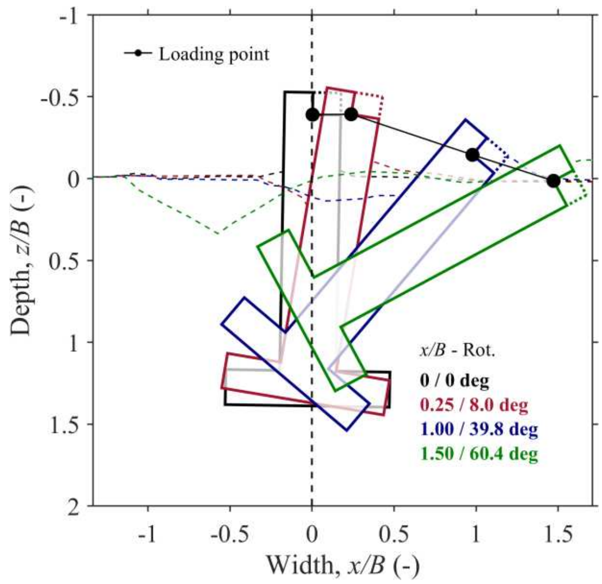

Figure 5. Evolution of anchor position and soil surface with progress of loading for HT2.

At the first peak ($x/B = 0.25$), the uplift and translation of the centre of the foundation base were minimal, while the rotation was 8.0°. At the second peak

(x/B = 1.5), the translation was limited, but the uplift and rotation (60.4°) were considerable.

Interestingly, the form of the load resistance profiles in Figure 4 is very similar to that observed during inclined loading (≤ 47° to the horizontal at the mudline) of the dynamically installed fish anchor (Chang et al., 2019; Kim et al., 2022). However, for fish anchor, this resistance profile was mobilised due to keying, followed by continually penetrating deeper into the soil (i.e. diving).

It should be noted that, generally, the resistance profiles for horizontally and vertically oriented plate anchors show a single peak, with the anchor translating and rotating (comparable to the keying process where the anchor orient itself towards the direction of the load) before reaching full mobilization and eventual pullout (e.g. Roy et al., 2022).

3.2 Mechanisms at first peak

The digital images captured by the micro camera close to the first peak (x/B = 0.25, see Figure 4) were analysed by PIV. The quantified displacement vectors and incremental shear strains γ_S (%) using 10 successive images (from $x/B = 0.25$ over a displacement of δ = 1 mm) are included in Figure 6.

With the progress of loading or rotation, in the loading side, the soil around the top (approximately) half length of the embedded shaft was pushed forward (Figure 6a). A rotational failure took place around the heel (front edge) of the anchor starting from the middle of the shaft to around ~0.7B of the anchor plate (with a scoop under the plate). In the rear or trailing side, the plate rotated with the soil above, with the rotation extended up to somewhat middle of the shaft.

Based on the formed shear bands (Figure 6b), a rotational slip line can be drawn from the middle of the front side of the shaft to around the edge of the heel, around the 0.7-0.9B of the base, and from the edge of the toe to the middle of the rear side of the shaft, and another triangular wedge shear line from the middle of the front side of the shaft to the soil surface.

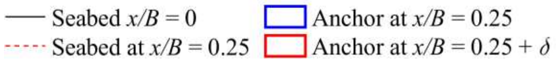

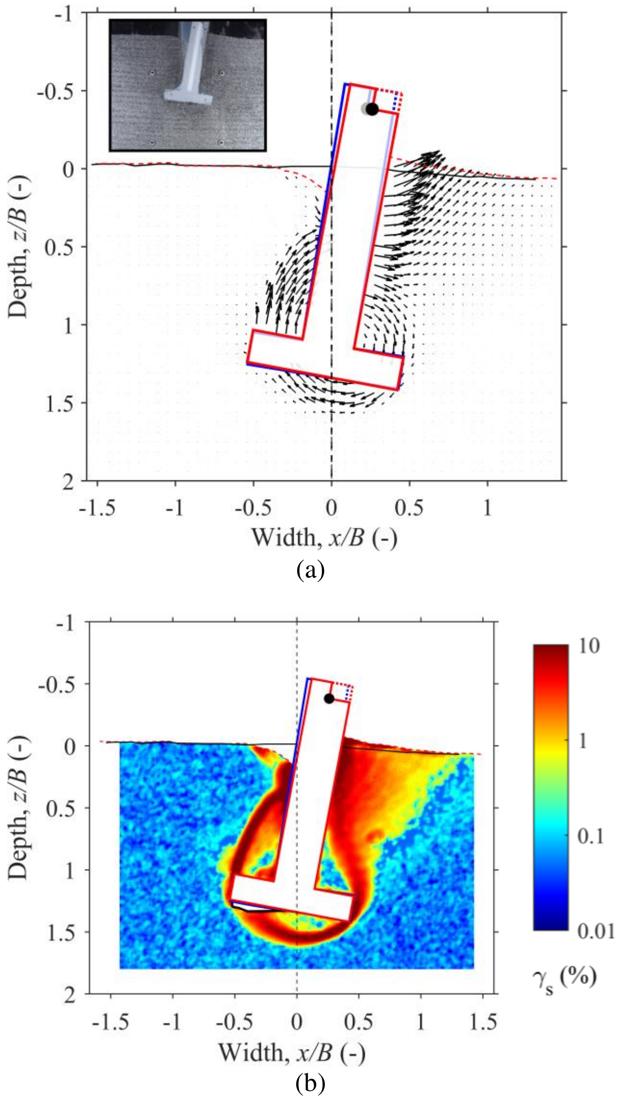

Figure 6. Mechanisms at first peak (x/B = 0.25) for HT2: (a) incremental displacement vectors; and (b) incremental shear strain fields.

3.3 Mechanisms at second peak

At the second peak (x/B = 1.5, see Figure 4), the soil above the toe lifted up, leading to formation of a perpendicular shear band from the edge of the toe to the soil surface (Figure 7). In the loading side, shear or frictional resistance also occurred along the front side of the shaft and heel. Sand continually caved in at the back or plate of the anchor.

It is anticipated that further work will comprehensively compare the failure mechanisms and capacity factors observed in this study with the existing data for horizontally and vertically oriented plate anchors in sand, discussing the effects of soil properties, loading direction, eccentricity, and anchor geometry

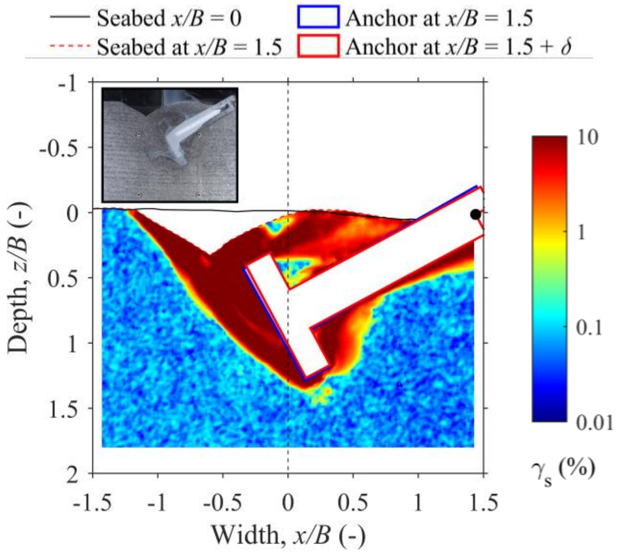

Figure 7. Incremental shear strain fields at second peak (x/B = 1.5) for HT2.

4 CONCLUSIONS

This paper presents a reverse T-shape square plate anchor that can be (i) used for station keeping of offshore floating wind turbines, wave energy converters, solar panels, and aquaculture cages; and (ii) potentially shared by two and four mooring lines from multiple floating units. The response of the anchor under uniaxial monotonic horizontal loading was primarily explored through full-model and half-model tests in a centrifuge. The tests were carried out in dry sand deposits, ensuring drained conditions, and varying sand relative density, and ground surface slope.

The load resistance profiles in very dense sand with flat ground surface, quantified by the full-anchor and half-anchor tests, exhibited four distinct load mobilisation phases. Two peaks appeared with the capacity at the 2nd peak being around two times that at the first one. The corresponding mobilised soil failure mechanisms (captured by the half-anchor tests and subsequently quantified by PIV analyses) were described illustrating incremental displacement vectors and shear strain fields. Analytical solutions and mechanism-based design approaches for estimating capacity under horizontal loading are being developed.

This study is now focusing on identifying a cost-effective method for installing the reverse T-shape anchor in the offshore environment. Subsequently, the effect of the installation process on the load-resistance profile will be investigated.

AUTHOR CONTRIBUTION STATEMENT

Pierre-Yves Duverneuil: Conceptualisation, Formal Analysis, Investigation, Writing – Original Draft. **Muhammad Shazzad Hossain**: Conceptualisation, Methodology, Supervision, Project Administration, Funding Aquisition, Writing – Review and Editing. **Henning Mohr**: Conceptualization, Investigation, Formal Analysis, Writing – Review and Editing. **Yun Sup Shin**: Review and Editing, Supervision.

ACKNOWLEDGEMENTS

The research presented here was undertaken with support from the consultancy research projects funded by Norwegian Geotechnical Institute (NGI). This support is gratefully acknowledged, as is the assistance of the centrifuge technicians, Manuel Palacios, Jason Stubbs, and Adam Stubbs.

REFERENCES

Cerfontaine, B., White, D. J., Kwa, K., Gourvenec, S. M., Knappett, J., & Brown, M. J. (2023). Anchor geotechnics for floating offshore wind: Current technologies and future innovations. *Ocean Engineering*, 279, 114327, doi.org/10.1016/j.oceaneng.2023.114327

Chang, K., Hossain, M. S., Wang, D., & Kim, Y. H. (2019). Performance of a novel dynamically installed fish anchor in calcareous silt. *Journal of Geotechnical and Geoenvironmental Engineering, ASCE*, 145(6), 04019019-1-14, doi.org/10.1061/(ASCE)GT.1943-5606.0002042

Kim, Y. H., Chow, S. H., Hossain, M. S., Zhao, J., & Rohan, S. (2022). Fish anchor diving behaviour: confirmation through field tests in the Swan River, *Géotechnique Letters*, 12(1), pp. 60-67, doi.org/10.1680/jgele.21.00007

Mohr, H., Gaudin, C. & Bransby M. F. (2022). The use of fibre optic and image analysis to investigate the performance of piles in sand under multi-directional horizontal loading, In: *Proceeeding of the 10th International Conference on Physical Modelling in Geotechnics (ICPMG2022)*, Daejeon, Korea.

Open Source Physics (2024). Tracker Video Analysis and Modeling Tool, Available at: https://www.compadre.org/osp/items/detail.cfm?ID=7365, accessed 11/11/2024.

Photron (2024). Automated motion analysis for 3D and 6D data requiring any single camera, Available at: https://photron.com/6d-marker/, accessed 13/11/2024.

Roy, A., O'loughlin, C. D., Chow, S. H., & Randolph, M. F. (2022). Inclined loading of horizontal plate anchors in sand. *Géotechnique*, 72(12), pp. 1051-1067, https://doi.org/10.1680/jgeot.20.P.119

Schneider, J. A., & Lehane, B. M. (2006). Effects of width for square centrifuge displacement piles in sand, In: *Proceedings of the 6th International Conference on Physical Modelling in Geotechnics (ICPMG06)*.

Stanier, S. A., Blaber, J., Take, W. A., & White, D. J. (2016). Improved image-based deformation measurement for geotechnical applications, *Canadian Geotechnical Journal,* 53(5), pp. 727-739, doi.org/10.1139/cgj-2015-0253

Stanier, S. A., & White, D. J. (2013). Improved image-based deformation measurement in the centrifuge environment, *Geotechnical Testing Journal*, 36(6), pp. 915–928, doi.org/10.1520/GTJ20130044

Subbulakshmi, A., Verma, M., Keerthana, M., Sasmal, S., Harikrishna, P., & Kapuria, S. (2022). Recent advances in experimental and numerical methods for dynamic analyses of floating offshore wind turbines - An integrated review. *Renewable and Sustainable Energy Reviews*, 164, doi.org/10.1016/j.rser.2022.112525

Teng, Y., Stanier, S. A., & Gourvenec, S. M. (2017). Synchronised multi-scale image analysis of soil deformations. *International Journal of Physical Modelling in Geotechnics*, 17(1), pp. 53-71, doi.org/10.1680/jphmg.15.00058

Xu, H., Rui, S., Shen, K., Jiang, L., Zhang, H., & Teng, L. (2024). Shared mooring systems for offshore floating wind farms: A review. *Energy Reviews*, 3(1), 100063, doi.org/10.1016/j.enrev.2023.100063

INTERNATIONAL SOCIETY FOR
SOIL MECHANICS AND
GEOTECHNICAL ENGINEERING

This paper was downloaded from the Online Library of the International Society for Soil Mechanics and Geotechnical Engineering (ISSMGE). The library is available here:

https://www.issmge.org/publications/online-library

This is an open-access database that archives thousands of papers published under the Auspices of the ISSMGE and maintained by the Innovation and Development Committee of ISSMGE.

The paper was published in the proceedings of the 5th International Symposium on Frontiers in Offshore Geotechnics (ISFOG2025) and was edited by Christelle Abadie, Zheng Li, Matthieu Blanc and Luc Thorel. The conference was held from June 9th to June 13th 2025 in Nantes, France.